

Magnetic Blue-Shift of Mott Gaps

Mohsen Hafez-Torbati,^{1,*} Davide Bossini,² Frithjof B. Anders,³ and Götz S. Uhrig^{1,†}

¹*Lehrstuhl für Theoretische Physik I, Technische Universität Dortmund, Otto-Hahn-Straße 4, 44221 Dortmund, Germany*

²*Department of Physics and Center for Applied Photonics, University of Konstanz, Konstanz, Germany*

³*Lehrstuhl für Theoretische Physik II, Technische Universität Dortmund, Otto-Hahn-Straße 4, 44221 Dortmund, Germany*

A substantial energy gap of charge excitations induced by strong correlations is the characteristic feature of Mott insulators. We study how the Mott gap is affected by the long-range antiferromagnetic order. Our key finding is that the Mott gap is enhanced by the magnetic ordering: a magnetic blue-shift (MBS) occurs. We establish this important and general effect in a three-dimensional Hubbard model, the paradigm for strongly correlated systems, without any spin-orbit term. The MBS is thus of exchange origin and can increase the Mott gap by approximately 70% as the temperature decreases from the ordering temperature to zero. The coupling between spin and charge degrees of freedom bears the potential to enable spin-to-charge conversion in Mott systems on extreme time-scales determined by the exchange only, since spin-orbit mediated transfer of angular momentum is not involved in the process. In view of spintronic and magnonic applications, we show that the magnetic contribution to the band-gap blue-shift observed in the optical conductivity of α -MnTe is correctly interpreted as the MBS of a Mott gap.

The discovery of insulating behavior in transition metal oxides [1] and its explanation in terms of strong electron-electron interaction [2] were the origin of the very active research field of strongly correlated systems ranging from Mott insulators [3–5] to high-temperature superconductors [6]. The low-energy physics of Mott insulators is governed by spin excitations [7]. A common and successful strategy to treat them consists in disentangling spin and charge degrees of freedom [8–11]. However, following this approach, it is difficult to track the coupling of charge and spin dynamics.

Recently a massive surge of interest in spintronics has involved antiferromagnetic materials [12], which are mostly Mott insulators [13–16]. The grand goal of this impressive research effort consists in establishing the ability to convert spin signals into charge responses. The typical approach relies on spin-orbit based transport effects, such as the spin Hall effect, requiring a heavy metal layer on top of the antiferromagnet to read out the electric system. The vision of a spintronic information technology based solely on antiferromagnetism, void of possible complication arising from the quality of the interface and unrestrained in its operational frequency, is fundamentally hampered by the lack of a general mechanism coupling spins to charges, which does not rely on the spin-orbit coupling. We note that the energy of the spin-orbit coupling sets the time-scale at which angular momentum can be transferred and the spin-charge conversion can take place. Therefore, we do not take the spin-orbit coupling into account.

Evidence has been reported that the charge gap in a Mott insulator, the Mott gap, depends on the magnetic ordering [17, 18]. Nevertheless, it is not clear whether this is an accidental feature of specific models or a generic characteristics of Mott insulators. In particular, a magnetic shift of the band gap could enable the coherent modulation of the current flowing through a transistor-type device, via the generation of magnons, which can be coherently induced [19, 20], even without laser-heating [21] and with frequencies above 20 THz [22–24].

Local electronic interactions are essential for the formation

of magnetic moments. Thus, there are two possible dichotomous scenarios for the influence of magnetic ordering on the charge gap: (i) the charge gap is a band gap of s and p electrons which are *different* from the electrons forming the magnetic degrees of freedom. Then, the influence of the localized spins is only indirect via superexchange with the itinerant electrons. (ii) the charge gap is a Mott gap so that the electrons forming the localized spins are also the ones forming the charge gap. In addition, a charge-transfer insulator also belongs to scenario (ii) because one of the bands relevant for the optical gap is a strongly correlated one.

So far, the observed magnetic shifts have been discussed in terms of scenario (i) [25–27]. This approach requires knowledge of many details of the systems and even the overall sign of the effect, red- or blue-shift, depends on them. Only very recently, the MBS in hexagonal MnTe (α -MnTe) has been associated to strong local interactions in a local static mean-field model [28]. In this Letter, we investigate the temperature dependence of the Mott gap across the transition from a paramagnetic insulator (PI) to an antiferromagnetic (AF) insulator. While the transition is best-known for the formation of a finite local spin-polarization m , we show that it is accompanied by a noticeable increase of the Mott gap, the magnetic blue-shift (MBS). First, we demonstrate the MBS in the three-dimensional (3D) Hubbard model as a paradigm for strongly correlated systems. We show that the Mott gap near the Néel temperature T_N can increase by about 70% upon reducing the temperature to zero.

Second, we analyze a specific system promising for applications, hexagonal MnTe (α -MnTe), which has been experimentally investigated [28, 29]. We extend the $S = 5/2$ spin model explaining the inelastic neutron scattering data [30, 31] to a Hubbard-Kondo model including charge degrees of freedom. We compute the MBS of the Mott gap of the half-filled $3d$ shell of Mn ions and show that it agrees with the MBS measured in the optical conductivity. Our findings set the stage to study coupled spin and charge dynamics in strongly correlated systems, including the specific case of α -MnTe.

The considered 3D Hubbard model at half-filling comprises hopping t between nearest-neighbor (NN) sites controlled by the parameter t and an interaction U between electrons at the same site with opposite spins

$$H = -t \sum_{\langle i,j \rangle} \sum_{\sigma=\uparrow,\downarrow} (c_{j,\sigma}^\dagger c_{i,\sigma} + \text{H.c.}) + U \sum_i n_{i,\downarrow} n_{i,\uparrow}. \quad (1)$$

The phase diagram at finite temperatures is well known [32]. At $T = 0$, the phase is a Néel antiferromagnet for any finite U/t [33], at high temperatures it is a metal for small U/t and a PI for large U/t separated from the metal by a crossover region. At large U/t the Mott gap is proportional to U because a charge excitation leads to the creation of a double occupancy.

We use dynamic mean-field theory (DMFT) which is an established approach for strong local interactions and large coordination number [3]. The frequency-dependent self-energy permits to describe paramagnetic Mott insulators, not accessible by static mean-field theories. We use the real-space DMFT (RDMFT) method [34–36] as implemented by one of us [37] and applied successfully to various models [38, 39]. Exact diagonalization (ED) is employed as impurity solver [40] allowing direct access to dynamics at real frequencies. The spectral function $A(\omega)$ results from the imaginary part of the local Green's function, averaged over both sublattice sites. We compute the Mott gap from the positions of the peaks in the spectral function. Although the spectral function for finite number of bath sites n_b consists of a series of sharp peaks approximating the continuous function, the Mott gap is found accurate and is used to benchmark the results of other methods [18]. We use the chemical potential μ to satisfy the half-filling condition. We study systems of $L \times L \times L$ sites with $L = 10$ and check for selected temperatures close to the transition that the results remain the same for $L = 20$.

In Figs. 1(a) and 1(b) we compare the spectral functions $A(\omega)$ in the magnetically ordered insulator (MI) and in the PI for $U = 20t$ and $n_b = 6$ bath sites in the impurity problem [41]. The spectral functions are shifted vertically for clarity. Lowering T in the PI hardly changes $A(\omega)$. But in the MI a shift of the electron and hole contributions to higher energies is observed. Below $T \approx 0.3t$ the stable phase is the MI, but the PI solution is given for comparison.

Figs. 1(c) and 1(d) depict the Mott gap in the PI and the MI as well as the local spin-polarization m in units of \hbar vs. the temperature T for $U = 15t$ (c) and $U = 20t$ (d). Results are displayed for two bath sizes, $n_b = 6$ and $n_b = 8$. For $U = 15t$, the gap in the PI changes slowly and for $U = 20t$ it is almost constant. However, in both cases there is a rapid increase of the gap upon entering the MI phase.

At the continuous transition from the PI to the MI the gaps have to be the same. This is not quite the case, most likely because of inaccuracies in extracting the gap from the ED data with finite bath sites. For $U = 15t$, the gap value is about $5.5t$ close to the transition temperature and rises to about $9.4t$ for $T \rightarrow 0$, i.e., it increases by about 70%. Comparing Figs. 1(c) and 1(d) a decrease of the MBS upon increasing U from $15t$

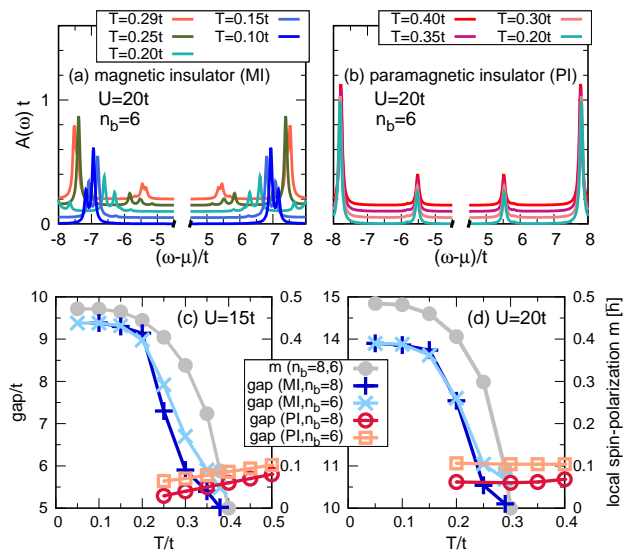


FIG. 1. The spectral function $A(\omega)$ vs. ω in the range $[-8t, +8t]$ at various temperatures T in the magnetically ordered insulator (MI) (a) and in the paramagnetic insulator (PI) (b) for $U = 20t$ and $n_b = 6$ bath sites in the impurity problem. The Mott gap vs. T in the MI and PI for $U = 15t$ in (c) and $U = 20t$ in (d). The grey lines show the local spin-polarization m (right axes).

to $20t$ is observed. Data for $U = 30t$ (not shown) indicates a continued reduction of the Mott gap.

The MBS is linked to the well-known decrease of the free-energy in the MI phase. The free-energy change below T_N is mainly due to the reduction of the internal energy, which can be determined solely from the single-particle spectral function. Upon transition from the PI to the MI a redistribution of the weight within the spectral function occurs which leads to a large increase in the internal energy if it is not compensated by a MBS, see Supplement Material A.

Next, we consider a specific experimental system, namely the magnetic semiconductor α -MnTe. It displays a noticeable additional increase of the optical gap below its Néel temperature $T_N \approx 310$ K. To separate the MBS from other temperature dependences the gap is fitted in the paramagnetic regime $T > T_N$ by the empirical Varshni function [42] which allows one to extrapolate the temperature dependence of the band gap in the absence of MBS down to zero temperature. The difference of the gap to the extrapolated value quantifies the MBS [28, 29]. Similar analyses were performed also for other magnetic semiconductors [25–27, 43].

The magnetic order in α -MnTe consists of planes of Mn^{2+} sites forming triangular lattices where spins are ferromagnetically ordered. These planes are stacked and the spins are oriented antiparallel between adjacent planes, originating the antiferromagnetic order. According to Hund's rule the spin at the Mn^{2+} sites is $S = 5/2$ due to the half-filled d -shell. The dispersion of the collective magnetic excitations is well understood [30, 31, 44]. On the other hand, the knowledge of the electronic excitations is significantly less developed and the

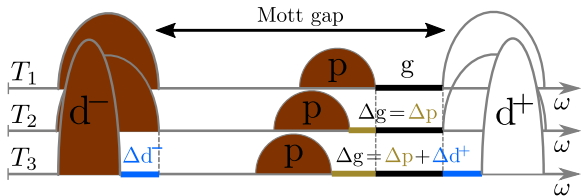


FIG. 2. Sketch of the bands in α -MnTe comprising the p bands at Te^{2-} and the lower (d^-) and upper (d^+) Hubbard bands of the $3d$ electrons at Mn^{2+} at three temperatures $T_1 > T_2 > T_N > T_3$, where T_N is the Néel temperature and g the optical gap. The energy difference between the d^- and the d^+ Hubbard bands defines the Mott gap while the optical gap is the difference between the p and the d^+ band, see main text.

understanding of its coupling to the magnetic system is still in its infancy. Density-functional calculations (DFT) [31, 45, 46] indicate that the conduction band in α -MnTe is dominated by Mn $3d$ contributions although the Mn $4s$ orbital is also involved. Assuming scenario (ii) to dominate we neglect the $4s$ admixture and treat MnTe as a charge-transfer insulator [16] where the optical gap g arises from promoting an electron from the filled p band of Te^{2-} to the empty upper Hubbard band d^+ on Mn^{2+} ; cf. the panel for T_1 in Fig. 2.

In addition, Fig. 2 schematically depicts the relative change of bands upon lowering the temperature $T_1 \rightarrow T_2 \rightarrow T_3$. As the temperature is decreased from T_1 to $T_2 > T_N$ the p and the d^+ bands shift apart. This increase of the band gap is induced by slight structural changes. It is continuous through the magnetic transition and thus captured by the extrapolation with the Varshni function. For $T_3 < T_N$ an additional contribution Δd^+ to the gap arises due to the MBS of the upper Hubbard band d^+ . In principle, the magnetic ordering could affect also the p band, but this would be indirect and we assume it to be less relevant. Consequently, we focus on the MBS and on an effective Hamiltonian describing the electrons in the $3d$ shell of the Mn^{2+} ions.

The established Heisenberg model for the spins at the Mn sites [30, 31] needs to be extended by the charge degrees of freedom. The full extension would require to consider five d bands at Mn sites plus three p bands at Te sites. This is by far too complex for an explicit numerical treatment of the strong interactions on the Mn sites. For this reason, we follow the idea proposed in Ref. [28] and describe the itineracy of each of the five d electrons in a one-band Hubbard model while treating the other four d electrons as localized forming a spin $S = 2$. We stress that the itinerant electron is a representative for all five electrons. We consider a Hubbard-Kondo lattice model on stacked triangular lattices, cf. Fig. 3,

$$H = - \sum_{i,j} \sum_{\sigma=\uparrow,\downarrow} t_{i,j} (c_{j,\sigma}^\dagger c_{i,\sigma} + \text{H.c.}) + U \sum_i n_{i,\downarrow} n_{i,\uparrow} - 2J_H \sum_i \vec{S}_i \cdot \vec{s}_i + \sum_{i,j} J_{i,j} (\vec{S}_i \cdot \vec{s}_j + \vec{S}_j \cdot \vec{s}_i + \vec{S}_i \cdot \vec{S}_j) \quad (2)$$

where J_H is the Hund coupling, \vec{S}_i the localized spin with

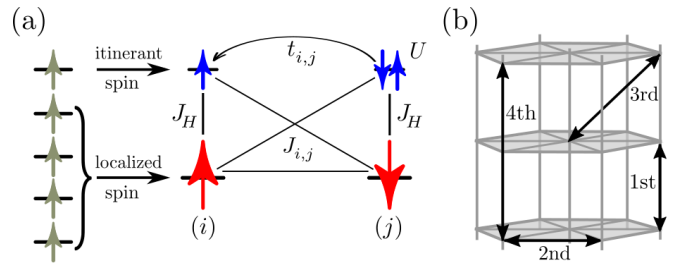


FIG. 3. (a) Illustration of the Hubbard-Kondo model (2) for the half-filled $3d$ shell of Mn ions at two sites i and j . (b) Stacked triangular layers with 1st, 2nd, 3rd, and 4th neighbor specified.

$S = 2$, and \vec{s}_i is the spin of the itinerant electron at site i . The local Hubbard repulsion is given by U , the $t_{i,j}$ are the hopping elements, and the $J_{i,j}$ the magnetic couplings, see Fig. 3(a).

The intersite couplings are limited to the four nearest neighbors specified in Fig. 3(b). We denote the hopping and the magnetic coupling of n th neighbor by t_n and J_n . The magnetic couplings are taken from the measured magnon dispersion [31] to be $J_1 = 3.072$ meV, $J_2 = 0.0272$ meV, $J_3 = 0.4$ meV, and $J_4 = 0.16$ meV, matching also the observed Néel temperature. The Hubbard interaction U ranges between ≈ 5 eV to ≈ 7 eV and the Hund coupling between ≈ 0.7 eV to ≈ 1.0 eV, based on estimates from atomic physics [28] and the DFT [31, 45] calculations. We investigate the effect of U and J_H on the MBS in this parameter regime. The hopping elements are determined such that they are consistent with the intersite exchange couplings, i.e., $J_n = 4t_n^2/\Delta$ where Δ is the bare charge gap $U + 4J_H$.

The DMFT accounts for the local interactions U and J_H . In the limit of infinite coordination number justifying DMFT, the intersite interactions J_n are properly treated by static mean-fields [47]. Thus, the intersite magnetic interactions are represented by

$$H_{\text{MF}} = - \sum_i (h_i^{\text{loc}} S_i^z + h_i^{\text{iti}} s_i^z) \quad (3)$$

where the effective magnetic field $h_i^{\text{loc}} = 2(J_1 - 3J_2 + 6J_3 - J_4)\langle S_i^z + s_i^z \rangle$ acts on the localized spin and $h_i^{\text{iti}} = 2(J_1 - 3J_2 + 6J_3 - J_4)\langle S_i^z \rangle$ on the itinerant electron; they are determined self-consistently [48]. The resulting Hamiltonian is solved using RDMFT [37] starting from an initial guess for the self-energy and the local magnetizations $\langle S_i^z \rangle$ and $\langle s_i^z \rangle$, which are updated in each RDMFT loop until the convergence is reached within some tolerance. The local impurity problem to be solved is a ferromagnetic Anderson-Kondo model with $S = 2$ [49] which takes the local electron-electron and electron-spin correlations into account [50].

For $U = 5.5$ eV and $J_H = 0.8$ eV Fig. 4(a) shows the spectral functions in the range -4.3 eV $\leq \omega \leq 4.3$ eV for various T obtained with $n_b = 5$ bath sites in the impurity problem. The spectral function remains almost unchanged in the paramagnetic phase $T \geq 379$ K in line with our findings

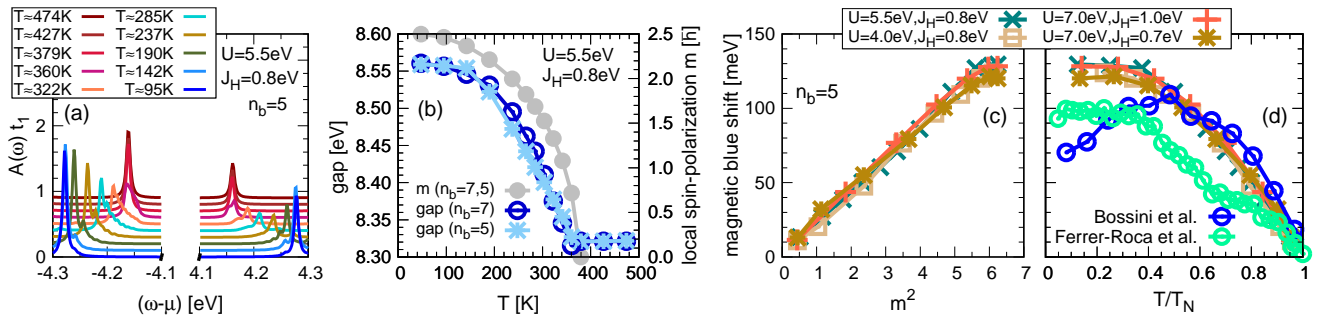


FIG. 4. (a) Spectral function $A(\omega)$ plotted for $\omega \in [-4.3, +4.3]$ eV for various T . (b) Gap and local spin-polarization m vs. T . (c,d) Theoretical results for the MBS in α -MnTe vs. the squared magnetization m^2 in (c) and vs. T/T_N in (d) for various values of U and J_H for $n_b = 5$. Panel (d) also displays the experimental data of Bossini et al. [28] and Ferrer-Roca et al. [29].

in the Hubbard model. Also, this result supports the above assumption that for $T > T_N$ the change of the gap is due to a relative shift of the p and the d^+ band, described by the Varshni fit. In the magnetically ordered phase for $T \leq 360$ K the peaks in the spectral function in Fig. 4(a) are shifted in energy. This shows that a significant MBS occurs also in the magnetic semiconductor α -MnTe underlining that the MBS is a wide-spread and generic phenomenon.

In Fig. 4(b) we plot the temperature dependence of the gap as obtained with $n_b = 5$ and $n_b = 7$ bath sites for the same values U and J_H as in Fig. 4(a). The agreement of both data sets underlines that the results do not depend on the number of bath sites. In addition, the local spin-polarization $m = |\langle S_i^z + s_i^z \rangle|$ is shown, coinciding for $n_b = 5$ and $n_b = 7$ and indicating a Néel temperature $T_N \approx 380$ K. This value represents a classical estimate since the DMFT approach does not capture intersite fluctuations which are shown [31] to reduce T_N to ≈ 310 K in accordance with experiment [44, 51, 52]. We expect the effect of the neglected intersite fluctuations on the gap to be of about 6 meV (≈ 70 K).

The magnetic AF ordering shown in Fig. 4(b) induces a MBS of about 250 meV which is the shift apart of the lower d^- and the upper d^+ Hubbard bands in Fig. 2, i.e., $\Delta d^+ + \Delta d^-$. Since we cannot calculate the individual contributions Δd^\pm separately, we assume they are shifted symmetrically, i.e., $\Delta d^+ = \Delta d^-$. This implies that the theoretical MBS is about 120 meV at its maximum. Fig. 4(c) shows that there is an almost linear relation between the squared local spin-polarization m^2 and the MBS for various parameter combinations of the local interactions U and J_H [53]. This behavior is in line with previous experimental [29] and theoretical [28] findings and, moreover, it underlines that the MBS is a robust effect not depending on details of the model.

Fig. 4(d) shows the MBS as function of T/T_N . For all four pairs of U and J_H we find the same Néel temperature $T_N \approx 380$ K. This underlines that T_N is determined by the intersite exchange couplings J_n which we kept fixed. But the Mott gap changes significantly from ≈ 7 eV for $U = 4.0$ eV and $J_H = 0.8$ eV to ≈ 11 eV for $U = 7.0$ eV and $J_H = 1.0$ eV. Despite this large change in the Mott gap there is hardly

any change in the MBS. This suggests that the MBS is determined only by the intersite exchange couplings and no other magnetic interaction, especially no spin-orbit coupling, are involved.

Fig. 4(d) also includes the experimental results for the MBS. The theoretical data are in striking agreement with the data of Bossini et al. [24] for $T \gtrsim 0.5T_N$. The data of Ferrer-Roca et al. are mentioned [29] to be probably underestimated between $T \approx 0.45T_N$ and $T \approx 0.65T_N$. The results of Bossini et al. deviate from theory below $T \approx 0.5T_N$ where the experimental data turn down unexpectedly. The origin of this deviating downturn is likely due to experimental reasons. We emphasize that the very good agreement between experiment and theory in Fig. 4(d) is achieved using generic parameters from literature without any fine-tuning. This provides strong evidence that the observed blue-shift upon ordering is the generic MBS of the advocated Hubbard-Kondo lattice model.

To summarize, we first considered the temperature dependence of the Mott gap in the paradigmatic Hubbard model. Clear evidence was found for a significant blue-shift upon lowering the temperature as soon as magnetic ordering sets in. We then elucidated the origin of the experimentally established MBS in α -MnTe as a promising candidate for applications with AF order at room temperature. We developed an extended Hubbard-Kondo lattice model displaying a temperature dependence of the blue-shift upon ordering in overall excellent agreement with the experimental findings for α -MnTe.

The presented results indicate that MBSs are generic in Mott insulators and can be found in a wide range of strongly correlated systems. In particular, strong MBSs in magnetic semiconductors can play a major role in spin-to-charge conversion even on ultrafast time-scale, since the effect is determined by intersite exchange interactions. Moreover, recent progress in the manipulation of antiferromagnetic magnons on ultrafast time scales [22, 54] add to the relevance of a comprehensive and quantitative understanding of the coupling of spin and charge dynamics [55]. Hence, the demonstrated MBS paves a promising route for future research, both fundamental and applied.

This study was funded by the German Research Foundation

(DFG) and the Russian Foundation for Basic Research in the International Collaborative Research Centre TRR 160 (Project B8) and by the DFG grant BO 5074/1-1.

* mohsen.hafez@tu-dortmund.de

† goetz.uhrig@tu-dortmund.de

- [1] J. H. de Boer and E. J. W. Verwey, *Proceedings of the Physical Society* **49**, 59–71 (1937).
- [2] N. F. Mott, *Proceedings of the Physical Society. Section A* **62**, 416 (1949).
- [3] A. Georges, G. Kotliar, W. Krauth, and M. J. Rozenberg, *Rev. Mod. Phys.* **68**, 13 (1996).
- [4] M. Imada, A. Fujimori, and Y. Tokura, *Rev. Mod. Phys.* **70**, 1039 (1998).
- [5] C. Giannetti, M. Capone, D. Fausti, M. Fabrizio, F. Parmigiani, and D. Mihailovic, *Advances in Physics* **65**, 58 (2016).
- [6] P. A. Lee, N. Nagaosa, and X.-G. Wen, *Rev. Mod. Phys.* **78**, 17 (2006).
- [7] E. Manousakis, *Rev. Mod. Phys.* **63**, 1 (1991).
- [8] P. Fazekas, *Lecture Notes on Electron Correlation and Magnetism*, Series in modern condensed matter physics (World Scientific, 1999).
- [9] A. Reischl, E. Müller-Hartmann, and G. S. Uhrig, *Phys. Rev. B* **70**, 245124 (2004).
- [10] S. A. Hamerla, S. Duffe, and G. S. Uhrig, *Phys. Rev. B* **82**, 235117 (2010).
- [11] M. Hafez-Torbati, N. A. Drescher, and G. S. Uhrig, *The European Physical Journal B* **88**, 3 (2015).
- [12] V. Baltz, A. Manchon, M. Tsoi, T. Moriyama, T. Ono, and Y. Tserkovnyak, *Rev. Mod. Phys.* **90**, 015005 (2018).
- [13] G. A. Sawatzky and J. W. Allen, *Phys. Rev. Lett.* **53**, 2339 (1984).
- [14] P. Němec, M. Fiebig, T. Kampfrath, and A. V. Kimel, *Nature Physics* **14**, 229 (2018).
- [15] A. Kirilyuk, A. V. Kimel, and T. Rasing, *Rev. Mod. Phys.* **82**, 2731–2784 (2010).
- [16] J. Zaanen, G. A. Sawatzky, and J. W. Allen, *Phys. Rev. Lett.* **55**, 418 (1985).
- [17] G. Sangiovanni, A. Toschi, E. Koch, K. Held, M. Capone, C. Castellani, O. Gunnarsson, S.-K. Mo, J. W. Allen, H.-D. Kim, A. Sekiyama, A. Yamasaki, S. Suga, and P. Metcalf, *Phys. Rev. B* **73**, 205121 (2006).
- [18] X. Wang, E. Gull, L. de’ Medici, M. Capone, and A. J. Millis, *Phys. Rev. B* **80**, 045101 (2009).
- [19] T. Satoh, S.-J. Cho, R. Iida, T. Shimura, K. Kuroda, H. Ueda, Y. Ueda, B. A. Ivanov, F. Nori, and M. Fiebig, *Phys. Rev. Lett.* **105**, 077402 (2010).
- [20] T. Kampfrath, A. Sell, G. Klatt, A. Pashkin, S. Mährlein, T. Dekorsy, M. Wolf, M. Fiebig, A. Leitenstorfer, and R. Huber, *Nature Photonics* **5**, 31 (2011).
- [21] D. Bossini, A. M. Kalashnikova, R. V. Pisarev, T. Rasing, and A. V. Kimel, *Phys. Rev. B* **89**, 060405 (2014).
- [22] D. Bossini, Dal Conte S., Hashimoto Y., Secchi A., Pisarev R. V., Rasing Th., Cerullo G., and Kimel A. V., *Nature Communications* **7**, 10645 (2016).
- [23] Y. Hashimoto, D. Bossini, T. H. Johansen, E. Saitoh, A. Kirilyuk, and T. Rasing, *Phys. Rev. B* **97**, 140404 (2018).
- [24] D. Bossini, S. Dal Conte, G. Cerullo, O. Gomonay, R. V. Pisarev, M. Borovsak, D. Mihailovic, J. Sinova, J. H. Mentink, T. Rasing, and A. V. Kimel, *Phys. Rev. B* **100**, 024428 (2019).
- [25] H.-h. Chou and H. Y. Fan, *Phys. Rev. B* **10**, 901 (1974).
- [26] J. Diouri, J. P. Lascaray, and M. E. Amrani, *Phys. Rev. B* **31**, 7995 (1985).
- [27] K. Ando, K. Takahashi, T. Okuda, and M. Umehara, *Phys. Rev. B* **46**, 12289 (1992).
- [28] D. Bossini, M. Terschanski, F. Mertens, G. Springholz, A. Bonanni, G. S. Uhrig, and M. Cinchetti, *New Journal of Physics* **22**, 083029 (2020).
- [29] C. Ferrer-Roca, A. Segura, C. Reig, and V. Muñoz, *Phys. Rev. B* **61**, 13679 (2000).
- [30] W. Szuszkiewicz, E. Dynowska, B. Witkowska, and B. Hennion, *Phys. Rev. B* **73**, 104403 (2006).
- [31] S. Mu, R. P. Hermann, S. Gorsse, H. Zhao, M. E. Manley, R. S. Fishman, and L. Lindsay, *Phys. Rev. Materials* **3**, 025403 (2019).
- [32] G. Rohringer, H. Hafermann, A. Toschi, A. A. Katanin, A. E. Antipov, M. I. Katsnelson, A. I. Lichtenstein, A. N. Rubtsov, and K. Held, *Rev. Mod. Phys.* **90**, 025003 (2018).
- [33] T. Pruschke and R. Zitzler, *Journal of Physics: Condensed Matter* **15**, 7867 (2003).
- [34] M. Potthoff and W. Nolting, *Phys. Rev. B* **59**, 2549 (1999).
- [35] Y. Song, R. Wortis, and W. A. Atkinson, *Phys. Rev. B* **77**, 054202 (2008).
- [36] M. Snoek, I. Titvinidze, C. Töke, K. Byczuk, and W. Hofstetter, *New Journal of Physics* **10**, 093008 (2008).
- [37] M. Hafez-Torbati and W. Hofstetter, *Phys. Rev. B* **98**, 245131 (2018).
- [38] M. Hafez-Torbati and W. Hofstetter, *Phys. Rev. B* **100**, 035133 (2019).
- [39] M. Hafez-Torbati, J.-H. Zheng, B. Irsigler, and W. Hofstetter, *Phys. Rev. B* **101**, 245159 (2020).
- [40] M. Caffarel and W. Krauth, *Phys. Rev. Lett.* **72**, 1545 (1994).
- [41] We point out that the spectral function does not depend on spin even in the MI due to the averaging over the sublattice sites.
- [42] Y. Varshni, *Physica* **34**, 149 (1967).
- [43] X. Zhu, Q. Lian, P. Zhang, W. Bai, K. Tang, L. Zhu, J. Yang, Y. Zhang, X. Tang, and J. Chu, *Opt. Lett.* **43**, 5547 (2018).
- [44] W. Szuszkiewicz, B. Hennion, B. Witkowska, E. Łusakowska, and A. Mycielski, *physica status solidi (c)* **2**, 1141 (2005).
- [45] S. J. Youn, B. I. Min, and A. J. Freeman, *physica status solidi (b)* **241**, 1411 (2004).
- [46] G. Yin, J.-X. Yu, Y. Liu, R. K. Lake, J. Zang, and K. L. Wang, *Phys. Rev. Lett.* **122**, 106602 (2019).
- [47] E. Müller-Hartmann, *Z. Phys. B* **74**, 507 (1989).
- [48] For simplicity, we take the magnetization in z -direction although a weak spin-orbit coupling orients it in x -direction [31, 46]. But for the isotropic model studied here this does not matter.
- [49] See Supplemental Materials for details.
- [50] R. Peters and T. Pruschke, *New Journal of Physics* **8**, 127 (2006).
- [51] K. Walther, *Solid State Communications* **5**, 399 (1967).
- [52] D. Kriegner, H. Reichlova, J. Grenzer, W. Schmidt, E. Ressouche, J. Godinho, T. Wagner, S. Y. Martin, A. B. Shick, V. V. Volobuev, G. Springholz, V. Holý, J. Wunderlich, T. Jungwirth, and K. Vyborny, *Phys. Rev. B* **96**, 214418 (2017).
- [53] The value of the gap at T_N is fixed such that the MBS in Fig. 4(c) vanishes at $m^2 \rightarrow 0$.
- [54] Bossini D., Konishi K., Toyoda S., Arima T., Yumoto J., and Kuwata-Gonokami M., *Nature Physics* **14**, 370–374 (2018).
- [55] K. Gillmeister, D. Golež, C. T. Chiang, N. Bittner, Y. Pavlyukh, J. Berakdar, P. Werner, and W. Widdra, *Nature Communications* **11**, 4095 (2020).

Supplemental Material: Magnetic Blue-Shift of Mott Gaps

Mohsen Hafez-Torbati,^{1,*} Davide Bossini,² Frithjof B. Anders,³ and Götz S. Uhrig^{1,†}

¹Lehrstuhl für Theoretische Physik I, Technische Universität Dortmund, Otto-Hahn-Straße 4, 44221 Dortmund, Germany

²Department of Physics and Center for Applied Photonics, University of Konstanz, Konstanz, Germany

³Lehrstuhl für Theoretische Physik II, Technische Universität Dortmund, Otto-Hahn-Straße 4, 44221 Dortmund, Germany

A) INTERNAL ENERGY AND MAGNETIC BLUE-SHIFT

The internal energy of a general interacting fermionic system described by the Hamiltonian

$$H = H_0 + W = \sum_{i,j} h_{i,j} c_i^\dagger c_j + \frac{1}{2} \sum_{i,j,k,l} W_{i,j,k,l} c_i^\dagger c_j^\dagger c_k c_l, \quad (1)$$

can be expressed as [1]

$$E := \langle H \rangle = \frac{1}{2} \sum_{i,j} \int_{-\infty}^{+\infty} d\omega A_{i,j}(\omega) f(\omega) [\omega \delta_{i,j} + h_{i,j}], \quad (2)$$

where i and j specify single-particle quantum numbers, $A_{i,j}(\omega)$ is the spectral function of the single-particle Green's function, and $f(\omega)$ is Fermi's function. Eq. (2) shows that the internal energy can be determined solely from the single-particle spectral function. The first contribution in Eq. (2) describes $\langle H_0 \rangle / 2 + \langle W \rangle$ and the second contribution is half of the kinetic energy, $\langle H_0 \rangle / 2$.

The Mott gap separating the lower and the upper Hubbard bands is typically much larger than the Néel temperature T_N . For temperatures $T \lesssim T_N$ this restricts the integration in Eq. (2) to only the lower Hubbard band (LHB). The first contribution in Eq. (2) for $T \lesssim T_N$ can be simplified as

$$\varepsilon_1 = \frac{E_1}{N} = \int_{\text{LHB}} \omega A(\omega) d\omega, \quad (3)$$

where N is the number of lattice sites and we used the translational symmetry of the spin-averaged local spectral function $A(\omega)$, which we plotted in Figs. 1(a,b) and Fig. 4(a) in the main text.

In order to see how the energy in Eq. (3) is distributed over the frequency we consider the partial energy

$$I(\omega) = \int_{-\infty}^{\omega} \omega' A(\omega') d\omega', \quad (4)$$

which equals ε_1 if ω is large enough to cover the whole LHB. In Fig. 1 we plot $I(\omega)$ for the 3D Hubbard model with $U = 15t$ and $T = 0.2t$ in the magnetic insulator (MI) and in the paramagnetic insulator (PI), as well as in the MI without any magnetic blue-shift (MBS) of the spectral function. The results are obtained using the number of bath sites $n_b = 6$ in the exact diagonalization impurity solver. Fig. 1 shows that upon transition from the paramagnetic to the magnetic phase a redistribution of the weight within the spectral function occurs which leads to a large increase in the internal energy if it is not compensated by a MBS.

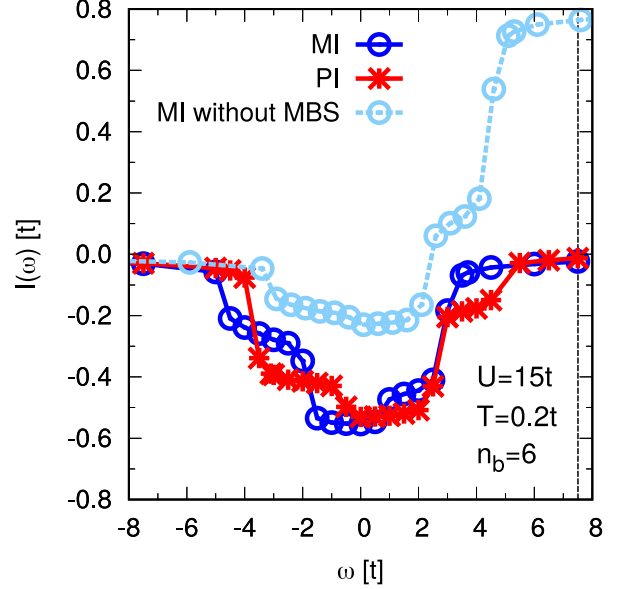


FIG. 1. The partial energy $I(\omega)$ defined by Eq. (4) versus frequency ω changing over the lower Hubbard band for the 3D Hubbard model with $U = 15t$ and $T = 0.2t$ in the magnetic insulator (MI) and in the paramagnetic insulator (PI) as well as in the MI without magnetic blue-shift (MBS) of the spectral function. The vertical dashed line at $U/2 = 7.5t$ specifies the Fermi energy. The number of bath sites $n_b = 6$ is used in the exact diagonalization impurity solver.

For the Hubbard model $H = H_t + H_U$ with the nearest-neighbor hopping term H_t and the Hubbard interaction H_U we plot the internal energy $\langle H_t + H_U \rangle$ per lattice site in Fig. 2 for $U = 15t$ and $n_b = 6$. We include also $\langle H_t/2 + H_U \rangle$ and $\langle H_t/2 \rangle$ corresponding to the first and the second contribution in Eq. (2), respectively. We see that $\langle H_t/2 + H_U \rangle$ remains close to zero and the reduction of the internal energy below T_N is mainly due to $\langle H_t/2 \rangle$. Without MBS the contribution $\langle H_t/2 + H_U \rangle$ would increase substantially in the MI phase, see Fig. 1. This shows that the MBS is crucial to achieve a decrease of the internal energy which is the prerequisite for the phase transition to occur.

B) DYNAMICAL MEAN-FIELD THEORY OF HUBBARD-KONDO MODEL

After the mean-field decoupling of the intersite magnetic couplings shown in Eq. (3) the Hamiltonian in Eq. (2) (both

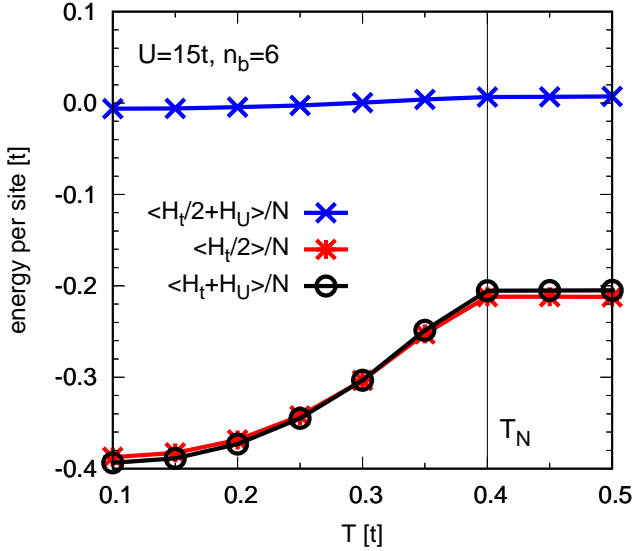


FIG. 2. The internal energy $\langle H_t + H_U \rangle$ and the individual contributions $\langle H_t/2 + H_U \rangle$ and $\langle H_t/2 \rangle$ of the Hubbard model $H = H_t + H_U$ per lattice site versus the temperature T for the Hubbard interaction $U = 15t$ and the number of bath sites $n_b = 6$ in the exact diagonalization impurity solver.

in the main text) reads

$$H = - \sum_{i,j} \sum_{\sigma} t_{j,i} \left(c_{j,\sigma}^{\dagger} c_{i,\sigma} + \text{H.c.} \right) - \sum_i \left(h_i^{\text{iti}} s_i^z + \mu n_i \right) + U \sum_i n_{i,\downarrow} n_{i,\uparrow} - 2J_H \sum_i \vec{S}_i \cdot \vec{s}_i - \sum_i h_i^{\text{loc}} S_i^z \quad (5)$$

with the effective magnetic fields

$$h_i^{\text{loc}} = 2(J_1 - 3J_2 + 6J_3 - J_4) \langle S_i^z + s_i^z \rangle, \quad (6a)$$

$$h_i^{\text{iti}} = 2(J_1 - 3J_2 + 6J_3 - J_4) \langle S_i^z \rangle \quad (6b)$$

acting on the localized spin \vec{S}_i and the spin of itinerant electrons \vec{s}_i , respectively, at the lattice site i . We added a chemical potential term μ to the Hamiltonian (5) to control the electron density $n_i := n_{i,\downarrow} + n_{i,\uparrow}$ in the system keeping it at half filling. In the derivation of Eq. (6) we consider ferromagnetic order within the triangular layers and antiferromagnetic order between them. For simplicity, the magnetic order is taken to be in the \hat{z} direction in spin space, but this assumption does not matter since we consider a fully spin isotropic model. The weak anisotropy stemming from a spin-orbit coupling [2, 3] is left to future research. The effective magnetic fields in Eq. (6) depend on the local spin-polarizations $\langle S_i^z \rangle$ and $\langle s_i^z \rangle$ and need to be determined self-consistently during the real-space dynamical mean-field theory (RDMFT) iteration.

We basically use the RDMFT implementation of Ref. [4] for SU(2) systems with a generalization of the Anderson impurity model to an Anderson-Kondo impurity model which includes additional local degrees of freedom such as the localized spin in Eq. (5). We also updated the implementation

of Ref. [4] such that some local expectation values are computed and output during the RDMFT loop so that mean-fields can be modified iteratively. In the case of the Hamiltonian (5) these local expectation values are the spin-polarizations $\langle s_i^z \rangle$ and $\langle S_i^z \rangle$, needed for the calculations of the effective magnetic fields Eq. (6). We stress that the local Green's function, the self-energy, and the dynamical Weiss field are all diagonal in spin space as the Hamiltonian Eq. (5) is diagonal in S^z . This simplifies the general formalism of Ref. [4].

The terms in the first line of Eq. (5) describe the non-interacting parts of the itinerant electrons from which the non-interacting lattice Green's function is constructed. The second line in Eq. (5) contains the Hubbard interaction between the itinerant electrons, the Hund coupling between the spin of the itinerant electron and the localized spin $S = 2$, and the effective magnetic field at the localized spin. They enter the calculation through the local impurity problem. The RDMFT loop starts with an initial guess for the self-energy matrix $\Sigma(i\omega_n)$ and the local spin-polarizations $\langle s_i^z \rangle$ and $\langle S_i^z \rangle$. The real-space lattice Green's function is calculated according to Dyson's equation

$$\mathbf{G}(i\omega_n) = [i\omega_n \mathbb{1} - \mathbf{H}_0 - \Sigma(i\omega_n)]^{-1} \quad (7)$$

where \mathbf{H}_0 is the matrix representation of the non-interacting terms in the first line of Eq. (5). To address the local problem at the lattice site i we use the Anderson-Kondo impurity model [5]

$$H_i = -\mu n_i - h_i^{\text{iti}} s_i^z + U n_{i,\downarrow} n_{i,\uparrow} - h_i^{\text{loc}} S_i^z - 2J_H \vec{S}_i \cdot \vec{s}_i + \sum_{\ell=1}^{n_b} \sum_{\sigma} \epsilon_{\ell}^i a_{\ell,\sigma}^{\dagger} a_{\ell,\sigma} + \sum_{\ell=1}^{n_b} \sum_{\sigma} \left(a_{\ell,\sigma}^{\dagger} V_{\ell,\sigma}^i c_{i,\sigma} + \text{H.c.} \right) \quad (8)$$

where $a_{\ell,\sigma}^{\dagger}$ and $a_{\ell,\sigma}$ are the fermionic creation and annihilation operators at the bath site ℓ with the spin $\sigma = \uparrow, \downarrow$. The bath sites in Eq. (8) approximate the effect of the surrounding sites in the lattice [6]. The bath parameters ϵ_{ℓ}^i and $V_{\ell,\sigma}^i$ are determined by fitting the dynamical Weiss field [4, 7]. The self-energy as well as the local spin-polarizations $\langle s_i^z \rangle$ and $\langle S_i^z \rangle$ are calculated using exact diagonalization of the Anderson-Kondo impurity model (8). They are employed for the next RDMFT iteration loop.

Since the model is symmetric with respect to a combined swap of the sublattice and the spin orientations, we only need to set up the impurity model (8) for one representative site. In this sense, the lattice solutions are homogeneous. Hence, one does not need to fully invert the matrix in Eq. (7) because only the two columns (due to the spin degree of freedom) corresponding to the representative site are needed [4]. This enables us to treat very large system sizes in Eq. (7) so that its finite-size corrections are completely negligible.

* mohsen.hafez@tu-dortmund.de

† goetz.uhrig@tu-dortmund.de

- [1] A. Fetter and J. Walecka, *Quantum Theory of Many-Particle Systems*, Dover Books on Physics (Dover Publications, 2012).
- [2] S. Mu, R. P. Hermann, S. Gorse, H. Zhao, M. E. Manley, R. S. Fishman, and L. Lindsay, *Phys. Rev. Materials* **3**, 025403 (2019).
- [3] G. Yin, J.-X. Yu, Y. Liu, R. K. Lake, J. Zang, and K. L. Wang, *Phys. Rev. Lett.* **122**, 106602 (2019).
- [4] M. Hafez-Torbati and W. Hofstetter, *Phys. Rev. B* **98**, 245131 (2018).
- [5] R. Peters and T. Pruschke, *New Journal of Physics* **8**, 127 (2006).
- [6] A. Georges, G. Kotliar, W. Krauth, and M. J. Rozenberg, *Rev. Mod. Phys.* **68**, 13 (1996).
- [7] M. Caffarel and W. Krauth, *Phys. Rev. Lett.* **72**, 1545 (1994).